Set Oriented Computation of Transport Rates in 3-degree of Freedom Systems: the Rydberg Atom in Crossed Fields

Michael Dellnitz*, Katalin A. Grubits†, Jerrold E. Marsden†,
Kathrin Padberg*, Bianca Thiere*

This version: May 17, 2005

Abstract

We present a new method based on set oriented computations for the calculation of reaction rates in chemical systems. The method is demonstrated with the Rydberg atom, an example for which traditional Transition State Theory fails. Coupled with dynamical systems theory, the set oriented approach provides a global description of the dynamics. The main idea of the method is as follows. We construct a box covering of a Poincaré section under consideration, use the Poincaré first return time for the identification of those regions relevant for transport and then we apply an adaptation of recently developed techniques for the computation of transport rates (Dellnitz, Junge, et al. [2005]; Padberg [2005]). The reaction rates in chemical systems are of great interest in chemistry, especially for realistic three and higher dimensional systems. Our method is applied to the Rydberg atom in crossed electric and magnetic fields. Our methods are complementary to, but in common problems considered, agree with, the results of Gabern, Koon, Marsden, and Ross [2005]. For the Rydberg atom, we consider both the half and full scattering problems in both the 2- and the 3-degree of freedom systems. The ionization of such atoms is a system on which many experiments have been done and it serves to illustrate the elegance of our method.

Contents

*Faculty of Computer Science, Electrical Engineering and Mathematics, University of Paderborn, 33095 Paderborn, Germany

†Control and Dynamical Systems, MC 107-81, California Institute of Technology, Pasadena, CA 91125, USA.

1 Introduction

One of the primary goals of chemical physics is the calculation of the rate at which a reaction proceeds. Transition State Theory (TST) (see e.g. Truhlar, Garrett, and Klippenstein [1996]), also known as Rice-Ramsperger-Kassel-Marcus (RRKM) theory (see e.g. Gilbert and Smith [1990]) is widely used in the chemistry community to calculate these rates. While successful in many examples, this statistical theory is inadequate in some other examples, and in those, it can have an error of a few orders of magnitude when compared with experimental results (De Leon [1992]).

TST identifies a transition state for the system under consideration; this is a set of states through which the reactants must pass in order to become products of the reaction. These transition states may be in phase space rather than configuration space but TST assumes that the regions in phase space connected by this transition state are structureless in the sense that motion within them is purely statistical (Marston and De Leon [1989]). However, in the examples where TST fails, this assumption breaks down and indeed, the structure of phase space must be accounted for when calculating reaction rates (Gabern, Koon, Marsden, and Ross [2005]).

De Leon, Mehta and Topper have shown, by developing reaction island theory, that cylindrical manifolds in phase space mediate two degree of freedom chemical reactions (De Leon, Mehta, and Topper [1991a], De Leon, Mehta, and Topper [1991b]). Uzer, Jaffé and co-workers have isolated some of the important geometrical aspects of the phase space structure for higher degree of freedom systems (Jaffé, Farrelly, and Uzer [1999], Uzer, Jaffé, Palacián, Yanguas, and Wiggins [2002]). We note that Koon, Lo, Marsden, and Ross [2000] emphasized the importance of heteroclinic networks and the associated cylindrical manifolds (tubes) when considering dynamical channels and Contopoulos and Efstathiou [2004] used escape rates from a surface of section to identify regions that govern the transport between parts of the phase space.

Gabern, Koon, Marsden, and Ross [2005] have calculated reaction rates in chemical systems with three degrees of freedom using dynamical systems tools and Monte Carlo methods. By taking into account the invariant manifold tubes that mediate the dynamics of a reaction, these rates were calculated for a system with non-statistical dynamics. A major difficulty that was overcome by using a Monte Carlo method was the calculation of the volume of the overlap of the invariant manifold tubes.

The present work uses a new approach, based on set oriented methods (see for example Dellnitz and Junge [2002]), to identify the structures in phase space that mediate chemical reactions and to calculate the associated reaction rates.

The set oriented approach focuses on a global description of the dynamics on a coarse level and covers the relevant region of phase space by appropriately sized boxes. By considering a transfer operator associated with the underlying map, one is able to describe the evolution of an initial distribution under the dynamics. Via a partition of some interesting region in phase space, this operator can be discretized, yielding a stochastic matrix. The transport rates between different regions in phase space can then be computed using this matrix of transition probabilities. This global analysis is more efficient and can provide more information than the calculation of many individual trajectories.

The primary differences between the approach presented in this paper and that of Gabern, Koon, Marsden, and Ross [2005] are that the set oriented method

1. does not use normal forms to find the invariant manifold tubes but rather uses information about the time trajectories take to return to a Poincaré section;

2. does not use Monte Carlo methods for the calculation of volumes as the necessary information is naturally given by the box volumes and the matrix of transition probabilities; and

3. does not use long term simulations but rather short term simulations for a large number of globally distributed initial particles.

Despite the large differences in methodology and computational tools, the results of the set oriented approach and that of Gabern, Koon, Marsden, and Ross [2005] are in good agreement, which gives one confidence in both methods.

The present paper takes the ionization of a Rydberg atom in crossed electric and magnetic fields as its example. Both the planar problem and the three dimensional problem are considered, with the half scattering and full scattering rates being calculated. The power and the potential of the set oriented approach in dealing with high-dimensional systems is thereby demonstrated.

In the following section, the physical background of the example considered in this paper is presented, followed by a detailed description of the model. Section 4 elucidates the set oriented method as it relates to the calculation of reaction rates. In section 5 the results are presented and discussed, followed in section 6 by conclusions and future directions.

2 Background

The Rydberg atom is a hydrogen-like atom in that it has one valence electron. Highly excited Rydberg atoms have enough energy such that the valence electron is far away from the nucleus and its dynamics can be treated classically, to a good approximation. Introducing external perpendicular electric and magnetic fields breaks the symmetry of the problem so that the escaping electron will do so in a particular direction. The escape of the electron from the field of the nucleus (and surrounding inner electrons) is known as ionization. The electron moves off to infinity and there is no possibility of return. This process is an example of a unimolecular reaction or dissociation.

The highly excited Rydberg atom is an interesting example not only because of its relation to other problems in chemical physics but also because of applications in diverse areas ranging from lasers to quantum computing (Federov and Ivanov [1990], Wojcik and Parzynski [1995], Ahn, Hutchinson, Rangan, and Bucksbaum [2001]). They are also of interest as they are at the overlapping region between classical and quantum mechanics, where the correspondence principle applies (Raithel and Walther [1994]). In addition to their theoretical interest, such atoms in crossed fields arise naturally in some astrophysical plasmas.

Rydberg atoms are a compelling test bed as they have a theoretical richness while also being experimentally accessible. Such atoms have been used to study the onset of classical chaos and to develop semi-classical models of quantum resonances (Marmet, Held, Raithel, Yeazell, and Walther [1994], De-Hua and Sheng-Lu [2004]). They are well suited to experiments as the internal field strengths of the atom are comparable to the external field strengths that are attainable in the laboratory (Raithel, Fauth, and Walther [1991]). Thus it is possible to study the strong-field regime.

Raithel, Walther and co-workers have studied Rydberg atoms in a number of arrangements, including the crossed fields arrangement. They have calculated ionization rates as a function of excitation energy for different values of the electric and magnetic fields (Raithel and Walther [1994]). Advances in experimental methods now allow the excitation of a Rydberg atom to a known energy level (Held, Schlichter, Raithel, and Walther [1998]). Thus, the techniques are available for experimentally calculating the ionization rates that are computed in the present paper. We certainly hope that the explicit experimental connection is achieved in the near future.

3 Model

3.1 Half and Full Scattering Problem

In a unimolecular dissociation reaction, the reactant is the bound state and the product is the unbound state. To pass from a bound state to an unbound state, the system must go through the transition state. Such reactions have come to be known as *half scattering problems* (Jaffé, Farrelly, and Uzer [1999]). The *full scattering*

problem involves moving through the transition state from an unbound state to a bound state and then back through the transition state to an unbound state. The example discussed in section 5 calculates rates of reaction for both the half scattering and full scattering problems.

The reaction will proceed only if the system has enough energy to overcome the energy barrier between reactants and products. For an energy at which the reaction can proceed, the energy in the system must find its way into a reactive mode for the reaction to occur. It is this process which determines the rate of the reaction.

These ideas are applied to the ionization of a highly excited Rydberg atom in external crossed electric and magnetic fields. Such an atom has an outer electron that is far enough away from the nucleus that its dynamics may be treated classically. This valence electron is assumed to have enough energy to pass through the transition state from the bound state to the unbound state, which is of course, ionization. Once in the unbound state, there is no possibility of return for the electron. This is the half scattering problem. The full scattering problem involves the *capture* of the electron followed by *ionization* of the same electron.

3.2 The Hamiltonian System

The dynamics of the electron is described classically by the following 3-degree of freedom Hamiltonian in co-ordinates that have been scaled by the cyclotron frequency:

$$H = \frac{1}{2}(p_x^2 + p_y^2 + p_z^2) - \frac{1}{r} + \frac{1}{2}(xp_y - yp_x) + \frac{1}{8}(x^2 + y^2) - \epsilon x, \tag{3.1}$$

where $r = \sqrt{x^2 + y^2 + z^2}$ is the distance between the electron and the center of the nuclear core. The cyclotron frequency, ω_c, is given by $\omega_c = eB/m$ where e is the electron charge, B is the magnetic field strength and m is the mass of the electron. The scaled electric field strength, ϵ, is defined by $\epsilon = \omega_c^{-4/3} E$ where E is the applied electric field strength (see for example Jaffé, Farrelly, and Uzer [1999]).

The Legendre transformation gives us the velocities

$$\dot{x} = p_x - \frac{y}{2}, \quad \dot{y} = p_y + \frac{x}{2}, \quad \dot{z} = p_z.$$

The Jacobi constant (first integral) is given by

$$C(x, y, z, \dot{x}, \dot{y}, \dot{z}) = -(\dot{x}^2 + \dot{y}^2 + \dot{z}^2) + 2\Omega(x, y, z) = -2E(x, y, z, \dot{x}, \dot{y}, \dot{z})$$

where

$$E(x, y, z, \dot{x}, \dot{y}, \dot{z}) = \frac{1}{2}(\dot{x}^2 + \dot{y}^2 + \dot{z}^2) - \Omega(x, y, z),$$

is the energy function. The effective potential function is $\Omega(x, y, z) = \epsilon x + \frac{1}{r}$. The 2-degree of freedom system is obtained by setting $z = \dot{z} = 0$ in the equations above.

The Stark saddle point occurs at

$$\begin{aligned} x &= \frac{1}{\sqrt{\epsilon}}, \quad y = 0\,, \quad z = 0, \\ \dot{x} &= 0\,, \quad \dot{y} = 0\,, \quad \dot{z} = 0. \end{aligned}$$

The Hill's region is the region of configuration space in which the electron is energetically forbidden to go and for $\dot{x} = \dot{y} = \dot{z} = 0$ is given by

$$M(\epsilon, C) = \{(x, y, z) \in \mathbb{R}^3 \mid \Omega(x, y, z) \geq C/2\}.$$

Figure 3.1(a) shows one of the possible cases of the Hill's region for the Rydberg atom projected onto the xy-plane. For some values of the energy (and hence C), the energetically forbidden region will be such that there is no way to go from a bound state to an unbound state or vice versa. That is, the neck region in the figure will close. Thus, for scattering problems we must have sufficient energy for the Hill's region to look qualitatively as shown in Figure 3.1(a).

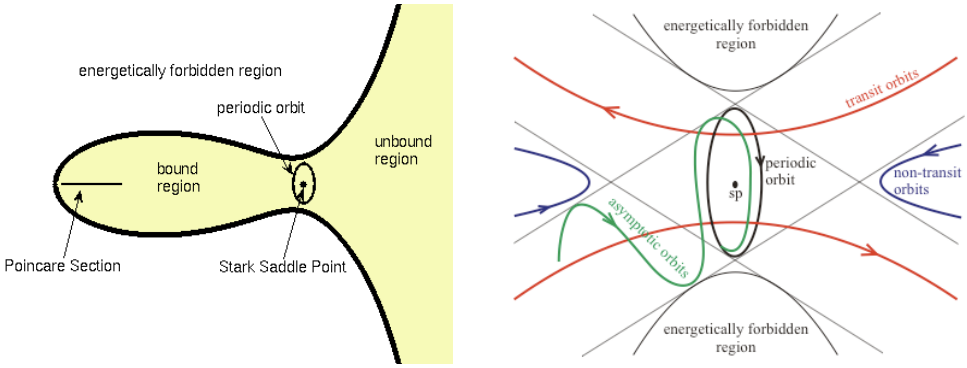

(a) (b)

Figure 3.1: (a) xy projection of the Hill's region (schematic). (b) The possible types of trajectories in the equilibrium region are shown in the xy projection (schematic). There are three different types of orbits: asymptotic (green), transit (red) and non-transit (blue) orbits (see Koon, Lo, Marsden, and Ross [2000]).

3.3 Dynamics Near the Saddle Equilibrium Point

For the computation of transition probabilities we need to identify regions in phase space that correspond to transport regions. In Transition State Theory the phase space associated with the reaction is traditionally assumed to be structureless (Marston and De Leon [1989]). Jaffé, Farrelly, and Uzer [1999], as well as Gabern, Koon, Marsden, and Ross [2005], have shown that this is not true for the problem of a Rydberg atom in crossed electric and magnetic fields. Their work builds on the work

of Conley [1968], McGehee [1969] and Koon, Lo, Marsden, and Ross [2000], which have shown this to also be true for the restricted three body problem in celestial mechanics.

For a system with n degrees of freedom, there is an invariant deformed $(2n-3)$-sphere that is the normally hyperbolic invariant manifold (NHIM), near the rank-one saddle equilibrium point sp. Orbits asymptotic to this sphere form the stable and unstable manifolds of the sphere. These manifolds (also called "tubes") are the key features of phase space that mediate transport through the transition state. As these tubes are $(2n-2)$ dimensional objects in a $(2n-1)$ dimensional energy surface, they divide the possible orbits into two categories: those that will pass through the transition state and those that will not. Orbits inside the stable manifold in the interior of the atom will pass through the transition state, that is, particles on these orbits will react. Figure 3.1(b) shows the possible types of trajectories in the region near the equilibrium point sp.

3.4 The Poincaré Section

To reduce the dimensionality, an appropriately chosen $(2n-2)$-dimensional Poincaré section is taken in the $(2n-1)$-dimensional energy surface. In our context of the 2- and 3-degree of freedom system we choose a Poincaré section Σ given by the conditions

$$y = 0, \quad x < 0, \quad \dot{y} > 0. \tag{3.2}$$

All of the essential dynamics are captured by the Poincaré section as trajectories will cross the Poincaré section only once in every loop that they make about the nuclear core at the origin. Thus we focus our attention on the dynamics on the Poincaré section.

In Figure 3.2 the xy-projection of typical (a) transit and (b) nontransit trajectories are shown. The starting point of the trajectory in (a) lies in the interior of the stable manifold tube and leaves the Poincaré section directly, whereas the starting point in (b) lies somewhere in the chaotic sea and comes back to Σ several times.

The first intersection of the unstable manifold tube with the Poincaré section contains those orbits that have just passed through the transition state from the unbound to the bound state. The forward mapping of these orbits under the Poincaré return map designates successive intersections of the unstable manifold tube with the Poincaré section. The first intersection of the stable manifold tube with the Poincaré section contains orbits that are about to pass through the transition state from the bound state to the unbound state. The m-th pre-image of this intersection under the Poincaré return map designates orbits that will pass through the transition state after m iterations. Thus in order to calculate rates of reaction for the half scattering problem, it is sufficient to find the transport probability into these intersections of the stable tube with the Poincaré section. For the computation of transport rates in the full scattering problem it is necessary to calculate transition probabilities between intersections of the stable and unstable manifold tubes with the Poincaré section. The methodology for these computations is explained in §4.

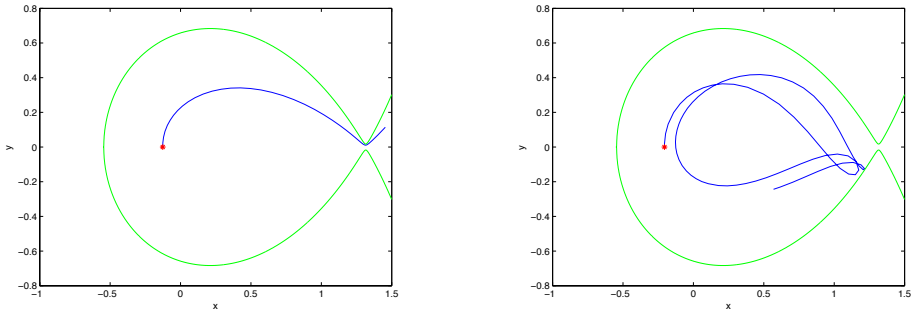

(a) (b)

Figure 3.2: Typical (a) transit and (b) nontransit trajectories. The xy projection of the Hill's region is shown in green. Compare with Figure 3.1.

All of our computations were with a fixed energy level of $E = -1.52$, which corresponds to a Jacobi constant of $C = 3.04$. With this value of energy, a reaction will be able to proceed if the electric field parameter is greater than $\epsilon = 0.5776$. If the scaled electric field is less than this value then the neck region between the bound and unbound states will be closed.

Figures 3.3 and 3.4 show the chaotic sea for the 2-degree of freedom Rydberg atom together with intersections of the stable (blue) and unstable (red) tube boundaries. The electric field parameter is $\epsilon = 0.57765$ for Figure 3.3, which is just above the critical value. Figure 3.3 (a) shows the first six intersections of the stable (blue) and unstable (red) tube boundaries with Σ and Figure 3.3 (b) focuses on the region of interest. These tube intersections are very thin in comparison to the intersections of the tube boundaries for $\epsilon = 0.58$ shown in Figure 3.4. The black dots in these diagrams represent trajectories crossing Σ. The same number of iterates and the same initial conditions were used for both values of ϵ. In both diagrams, the inside of the first intersection of the unstable tube with Σ is white because particles of this region will be mapped out of this region under one iteration of the map and no particles of the initial distribution will be mapped into this region. For an electric field parameter $\epsilon = 0.57765$, if a particle's trajectory begins in the unstable (red) tube, it will take five iterations before it could possibly be in the stable (blue) tube. Thus in the full scattering problem, once an electron has been captured, it will make five loops about the nuclear core before it could possibly leave the atom. For an electric field parameter $\epsilon = 0.58$, the first unstable tube intersection with Σ already overlaps the first stable tube intersection.

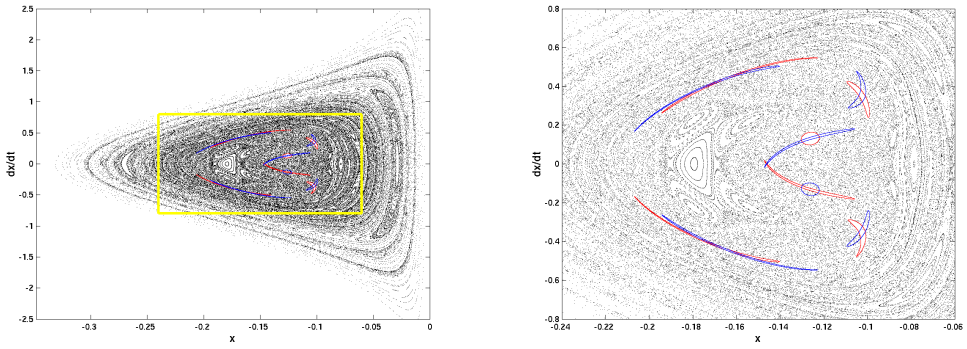

(a) (b) zoom into (a)

Figure 3.3: Chaotic sea for the 2-degree of freedom Rydberg atom is shown with the first six intersections of the unstable (red) and stable (blue) tube boundaries with the Poincaré section Σ under consideration. For this electric field parameter of $\epsilon = 0.57765$, the neck between the bound and unbound region is only open a little.

4 Set Oriented Methods

In this section we describe the general methodology for the computation of transition probabilities. We first introduce a method for the identification of the regions we are interested in. We then discuss a technique for the computation of transport rates and probabilities. It makes use of an appropriate discretization of a transfer operator. Both of these methods are based on the set oriented approach (see for instance Dellnitz and Hohmann [1996, 1997], Dellnitz and Junge [2002]).

4.1 Computation of Tube Intersections with Σ

As mentioned earlier, to compute the transition rate for the half and full scattering problems, one needs to identify the intersections of the stable and unstable manifolds with the Poincaré section Σ. One possible way is described in Gabern, Koon, Marsden, and Ross [2005] and the references therein. The authors use a normal form method for the computation of the stable and unstable manifolds and their intersection with Σ.

We follow a different approach to compute the intersections. We build on the concepts of Mezić and Wiggins [1999]. They use an algorithm for a decomposition of the phase space into those invariant sets on which the corresponding dynamical system is ergodic. Based on these ideas, we develop a multilevel approach for the decomposition of the set of interest.

First Return Time. Consider the system $\dot{x} = g(x)$ with $x \in \mathbb{R}^d$ and a smooth function $g : \mathbb{R}^d \to \mathbb{R}^d$. Then the vector field g generates a flow $\varphi^t : \mathbb{R}^d \to \mathbb{R}^d$ with a

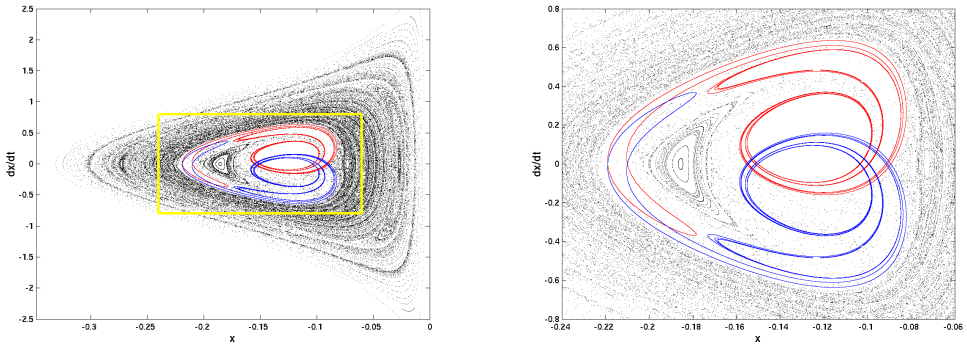

(a) (b) zoom into (a)

Figure 3.4: Chaotic sea for the 2-degree of freedom Rydberg atom for an electric field parameter of $\epsilon = 0.58$. The first three intersections of the unstable (red) and stable (blue) tube boundaries with the Poincaré section Σ under consideration are shown in (a), whereas (b) is a zoom into the interesting region of (a).

smooth function φ defined for all $x \in \mathbb{R}^d$ and t in some interval $I \in \mathbb{R}$. Consider a local compact cross section $\Sigma \subset \mathbb{R}^d$ which is transverse to the flow φ, and each point $q \in \Sigma$ has to be valid in the system g. Recall that the *Poincaré map* $P : U \to \Sigma$ for a point $q \in U$ is defined by $P(q) = \varphi^{\tilde{\tau}(q)}(q)$, where $U \subseteq \Sigma$ and $\tilde{\tau}(q)$ is the time taken for the orbit $\varphi^{\tilde{\tau}(q)}(q)$ which starts at q to first return to Σ. We call $\tilde{\tau}(q)$ the *first return time* (see for example Guckenheimer and Holmes [1983]).

We make use of the return time to divide the section Σ into different regions. Therefore, we need to define $\tilde{\tau}(q)$ for all $q \in \Sigma$ even if points do not come back to Σ. If $U = \Sigma$ then all points of the Poincaré section Σ will come back to it by definition and $\tilde{\tau}(q)$ exists for all $q \in \Sigma$. If $U \subset \Sigma$ then there are points in $\Sigma \backslash U$ for which the Poincaré map P is not defined. For our analysis, it is necessary that all points in Σ are assigned a time. Therefore, we define

$$\tau(q) := \begin{cases} \tilde{\tau}(q) : & q \in U \\ \infty : & q \in \Sigma \backslash U. \end{cases} \tag{4.1}$$

We use definition (4.1) for the computation of the first stable and unstable tube intersections with Σ. Figure 4.1 shows the first return time distribution for the 2-degree of freedom Rydberg atom in crossed electric and magnetic fields for an electric field parameter $\epsilon = 0.58$. For this we took the rectangle $X = [-0.295, -0.005] \times [-1.0, 1.0]$ as Σ and divided it into 16384 small boxes. The coloring of the boxes corresponds to the average return time with respect to initial conditions in the respective box. Dark blue indicates a short average return time and dark red an infinite return time. The dark red region corresponds to the interior and the boundary of the stable tube (compare with Figure 3.4).

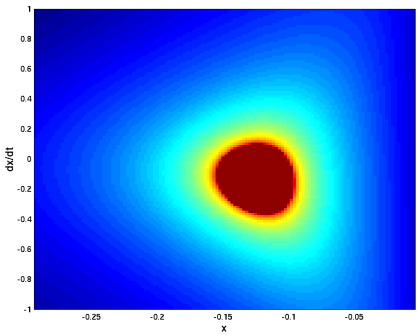

Figure 4.1: First return time distribution of the rectangle $X = [-0.295, -0.005] \times [-1.0, 1.0]$ for an electric field parameter $\epsilon = 0.58$. The color scheme goes from dark blue, indicating that the return time is very short, up to dark red where the points do not come back to the Poincaré section under consideration.

In section 3.3 we introduced asymptotic, transit and nontransit orbits, which we will denote by $\mathcal{O}_{as}$, $\mathcal{O}_{tr}$ and $\mathcal{O}_{ntr}$, respectively. These are orbits on the boundary, inside and outside of the invariant manifolds respectively. Uniqueness of solutions ensures that an orbit cannot change between these groups (see Gabern, Koon, Marsden, and Ross [2005]; Koon, Lo, Marsden, and Ross [2000]).

Recall that there is no possibility of return for the valence electron after it crosses from the bound to the unbound state. This means that for the system under consideration, particles that leave the Poincaré section through the interior of the first intersection of the stable manifold with Σ will never come back to Σ. The same applies to particles on the boundary of this intersection. Therefore, in terms of return times, the sets $\mathcal{O}_{as}$, $\mathcal{O}_{tr}$ and $\mathcal{O}_{ntr}$ are given by

$$\begin{aligned}
\mathcal{O}_{as} &= \{x \in \Sigma \mid \exists\, \epsilon > 0 \text{ and } \exists\, y, z \in V_\epsilon(x) \text{ with } \tau(y) = \infty \text{ and } \tau(z) < \infty\},\\
\mathcal{O}_{tr} &= \{x \in \Sigma \mid \exists\, \epsilon > 0 \text{ such that } \forall y \in V_\epsilon(x), \tau(y) = \infty\},\\
\mathcal{O}_{ntr} &= \{x \in \Sigma \mid \exists\, \epsilon > 0 \text{ such that } \forall y \in V_\epsilon(x), \tau(y) < \infty\},
\end{aligned}$$

where $V_\epsilon(x)$ denotes an ϵ-neighborhood of x.

With these theoretical considerations we are now able to devise an algorithm, which is based on the ideas of Dellnitz and Hohmann [1996, 1997] and provides a method for the approximation of $\mathcal{O}_{as}$.

Set Oriented Subdivision Algorithm. The set oriented *subdivision algorithm* generates a sequence $\mathcal{B}_0, \mathcal{B}_1, \ldots$ of finite collections of compact subsets of $\mathbb{R}^n$ such that the diameter $\operatorname{diam}(\mathcal{B}_k) = \max_{B \in \mathcal{B}_k} \operatorname{diam}(B)$ converges to zero for $k \to \infty$. Given an initial collection $\mathcal{B}_0$, we obtain $\mathcal{B}_k$ from $\mathcal{B}_{k-1}$ for $k = 1, 2, \ldots$ by

(i) *Subdivision:*
Construct a new collection $\hat{\mathcal{B}}_k$ such that

$$\bigcup_{B\in\hat{\mathcal{B}}_k} B = \bigcup_{B\in\mathcal{B}_{k-1}} B \text{ and}$$

$$\operatorname{diam}(\hat{\mathcal{B}}_k) \le \theta_k \operatorname{diam}(\mathcal{B}_{k-1}) \text{ where } 0 < \theta_{min} \le \theta_k \le \theta_{max} < 1.$$

(ii) *Selection:* Define a new collection $\mathcal{B}_k$ by

$$\mathcal{B}_k = \{B \in \hat{\mathcal{B}}_k \mid \exists\, x, y \in B \text{ with } \tau(x) = \infty \text{ and } \tau(y) < \infty\}.$$

Remark. By construction we have

$$\operatorname{diam}(\mathcal{B}_k) \le \theta_{max}^k \operatorname{diam}(\mathcal{B}_0) \to 0 \text{ for } k \to \infty.$$

We denote by Σ_k the collection of compact subsets obtained after k subdivision steps, $\Sigma_0 = \Sigma$. These Σ_k's define a nested sequence of compact sets, i.e. $\Sigma_{k+1} \subset \Sigma_k$. For each l we have $\Sigma_l = \bigcap_{k=0}^{l} \Sigma_k$, and we may view

$$\Sigma_\infty = \bigcap_{k=0}^{\infty} \Sigma_k$$

as the limit of the Σ_k's.

Obviously, this algorithm converges to

$$\mathcal{O}_{as} = \Sigma_\infty.$$

Remark. To obtain the sets corresponding to the unstable manifold one needs to proceed backwards in time.

For the 3-degree of freedom system and a parameter value of $\epsilon = 0.58$, Figure 4.2 shows the $x\dot{x}$- and $z\dot{z}$-projections of the first stable (blue) and first unstable (red) tube intersections.

Higher Return Times. The concept of the computation of the first tube intersection with the Poincaré section can easily be extended to the computation of further intersections. The n-th return time to Σ is denoted by $\tau^n(q)$ for $q \in \Sigma$. Figures 3.3 and 3.4 show further intersections of the stable (blue) and unstable (red) tube boundaries with Σ for two different parameter values. These computations were carried out using the above subdivision algorithm.

Now we have identified and approximated the regions of interest – for the following transport computations we only need the first intersections of the stable and unstable manifold with the Poincaré section. In the next subsection we show how the transition rates between these sets can be computed.

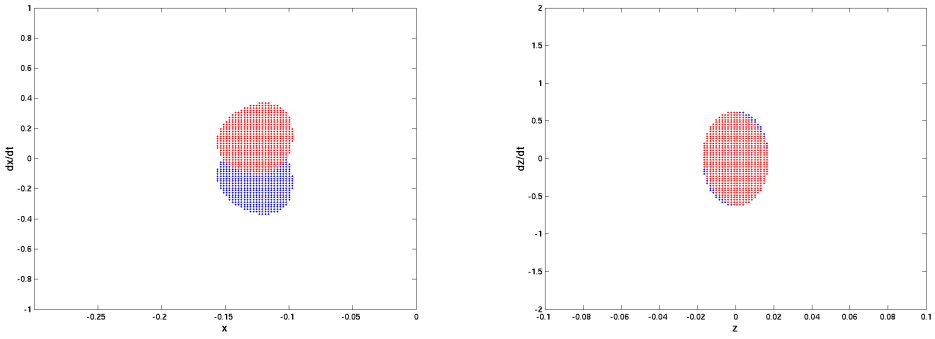

(a) (b)

Figure 4.2: First intersection of the stable (blue) and unstable (red) tube with the Poincaré section in (a) $x\dot{x}$- and (b) $z\dot{z}$-projections for a parameter value $\epsilon = 0.58$.

4.2 Transport Rates

The set oriented approach provides a convenient framework for the computation of transport rates between regions of interest. In the following, we briefly describe a method that relies on an appropriate discretization of a transfer operator – the Perron-Frobenius operator. For a detailed description we refer to Dellnitz, Junge, et al. [2005] and Padberg [2005].

Transfer Operator. Let

$$f : M \to M, \quad x_{k+1} = f(x_k), \quad k \in \mathbb{Z},$$

be a map and $R_1, \dots R_l \subset M$ a partition of M into l regions. We are interested in the transport rates

$$T_{i,j}(n) = m(f^{-n}(R_j) \cap R_i),$$

where m denotes the Lebesgue measure, that is, the mass or volume of material transported from some region R_i to R_j in n steps.

Generally, the evolution of measures ν on M can be described in terms of the *transfer operator* (or *Perron–Frobenius operator*) associated with f. This is a linear operator $P : \mathcal{M} \to \mathcal{M}$,

$$(P\nu)(A) = \nu(f^{-1}(A)), \quad A \text{ measurable},$$

on the space $\mathcal{M}$ of signed measures on M.

This operator concept relates to the transport quantities in the following way:

Corollary 4.1. *Let $m_i \in \mathcal{M}$ be the measure $m_i(A) = m(A \cap R_i) = \int_A \chi_{R_i}\, dm$, where χ_{R_i} denotes the indicator function on the region R_i. Then*

$$T_{i,j}(n) = (P^n m_i)(R_j).$$

(Here P^n refers to the n-fold application of the transfer operator P.)

Since an analytic expression for this operator will usually not be available, we need to derive a finite-dimensional approximation to it.

Discretization of Transfer Operators. As a finite dimensional space $\mathcal{M}_\mathcal{B}$ of measures on M we consider the space of absolutely continuous measures with density $h \in \Delta_\mathcal{B} := \text{span}\{\chi_B \mid B \in \mathcal{B}\}$, i.e. one which is piecewise constant on the elements of the partition (box covering) $\mathcal{B}$. Let $Q_\mathcal{B} : L^1 \to \Delta_\mathcal{B}$ be the projection

$$Q_\mathcal{B} h = \sum_{B \in \mathcal{B}} \frac{1}{m(B)} \int_B h \, dm \, \chi_B.$$

Then for every set A that is the union of partition elements we have

$$\int_A Q_\mathcal{B} h \, dm = \int_A h \, dm.$$

Hence a discretization of the transfer operator P with respect to the box collection $\mathcal{B}$, consisting of b boxes, is given in terms of a transition matrix $P_\mathcal{B} := (p_{ij})$ with

$$p_{ij} = \frac{m(f^{-1}(B_i) \cap B_j)}{m(B_j)}, \quad i, j = 1, \ldots, b.$$

So the entry p_{ij} gives the (conditional) probability that a particle is mapped from box B_j to B_i within one iterate of f.

Approximation of Transport Rates. For a measurable set A let

$$\underline{A} = \bigcup_{B \in \mathcal{B} : B \subset A} B \quad \text{and} \quad \overline{A} = \bigcup_{B \in \mathcal{B} : B \cap A \neq \emptyset} B.$$

We obtain the following estimate on the error between the true transport rate $T_{i,j}(n)$ and its approximation using powers of the transition matrix $P_\mathcal{B}$. To abbreviate notation, let $\underline{e_R}, \overline{e_R}, \underline{u_R}$ and $\overline{u_R} \in \mathbb{R}^b$ be defined by

$$(\underline{e_R})_i = \begin{cases} 1, & \text{if } B_i \subset R \\ 0, & \text{else} \end{cases}, \quad (\overline{e_R})_i = \begin{cases} 1, & \text{if } B_i \cap R \neq \emptyset \\ 0, & \text{else} \end{cases}$$

and

$$(\underline{u_R})_i = \begin{cases} m(B_i), & \text{if } B_i \subset R \\ 0, & \text{else} \end{cases}, (\overline{u_R})_i = \begin{cases} m(B_i), & \text{if } B_i \cap R \neq \emptyset \\ 0, & \text{else} \end{cases}$$

where $i = 1, \ldots, b$.

Lemma 4.2. *Let $R_i, R_j \subset M$,*

$$S_0 = R_j, \quad S_{k+1} = f^{-1}(\overline{S_k}), \quad k = 0, \ldots, n-1$$

and

$$s_0 = R_j, \quad s_{k+1} = f^{-1}(\underline{s_k}), \quad k = 0, \ldots, n-1.$$

Then

$$\begin{aligned}
&\left| T_{i,j}(n) - \underline{e_{R_j}}^T P_{\mathcal{B}}^n \, \underline{u_{R_i}} \right| \\
&\leq \underline{e_{R_j}}^T P_{\mathcal{B}}^n (\overline{u_{R_i}} - \underline{u_{R_i}}) + (\overline{e_{R_j}} - \underline{e_{R_j}})^T P_{\mathcal{B}}^n \overline{u_{R_i}} \\
&+ \max \left\{ m\left(f^{-n}(R_j \setminus \underline{R_j}) \cap R_i \right), m\left(f^{-n}(\overline{R_j} \setminus R_j) \cap R_i \right) \right\} \\
&+ \max \left\{ m\left((S_n \setminus f^{-n}(\underline{R_j})) \cap R_i \right), m\left((f^{-n}(\overline{R_j}) \setminus s_n) \cap R_i \right) \right\}.
\end{aligned}$$

For a proof of this statement we refer to Padberg [2005]. This result is an improvement of a similar estimate in Dellnitz, Junge, et al. [2005]. The main difference is that in our statement the error stays bounded if n goes to infinity. Furthermore, this estimate gives a bound on the error between the true transport rate $T_{i,j}(n)$ and the one computed via the transition matrix $P_{\mathcal{B}}$. Especially those elements of the fine partition $\mathcal{B}$ contribute to the error which either intersect the boundaries or which contain preimages of the boundary of R_j, see Figure 4.3 for an illustration. An obvious consequence of Lemma 4.2 is that in order ensure a certain degree of accuracy of the transport rates, these particular boxes need to be refined.

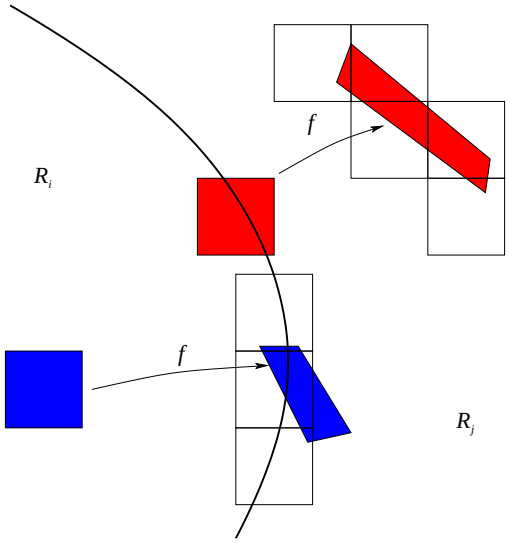

Figure 4.3: Two box transitions that contribute to the error between the computed and the actual value of the transport rate from a region R_i into region R_j after one iterate. Picture taken from Dellnitz, Junge, et al. [2005].

Convergence. Using Lemma 4.2 one can prove convergence for the approximate transport rate as the box covering is refined, see Dellnitz, Junge, et al. [2005] and Padberg [2005].

Adaptive Refinement of the Box Covering. As shown above, the boxes that contribute considerably to the error are those that either map onto the boundary

of the target set or whose preimage lies on the boundary of the source set. Unlike the situation in Dellnitz, Junge, et al. [2005], one usually does not observe the desired transport within one iteration of the map, but only after a longer time span. Therefore, we use the following algorithm, discussed in Padberg [2005], for the refinement of the transport boxes.

Adaptive Algorithm. Let $R_i, R_j \subset M$ and $n \in \mathbb{N}$. Let $\mathcal{B}$ be a box covering of M, let $N := \lceil \frac{n}{2} \rceil$ and let $P_{\mathcal{B}}$ be the transition matrix as defined above. Determine the boundary boxes

$$b_{R_i} := \overline{R_i} \setminus \underline{R_i}$$
$$b_{R_j} := \overline{R_j} \setminus \underline{R_j}$$

and compute

$$\underline{T_{i,j}(n)} := \underline{e_{R_j}}^T P_{\mathcal{B}}^n \, \underline{u_{R_i}}$$
$$\overline{T_{i,j}(n)} := \overline{e_{R_j}}^T P_{\mathcal{B}}^n \, \overline{u_{R_i}},$$

the *numerical* lower and upper bound on the transport rate $T_{i,j}(n)$ respectively. Choose $J \in \mathbb{N}$.

For $j = 1, \ldots, J$

1. Mark all boxes B for which

$$f_k(B) \cap b_{R_j} \neq \emptyset \text{ for } k \in \{1, \ldots, N\}$$

or

$$f^{-k}(B) \cap b_{R_i} \neq \emptyset \text{ for } k \in \{1, \ldots, N\}.$$

(This information is coded in the transition matrix.)

2. Subdivide marked boxes.
3. Compute $P_{\mathcal{B}}$.
4. Determine b_{R_i}, b_{R_j}, $\underline{T_{i,j}(n)}$, and $\overline{T_{i,j}(n)}$.

The algorithm produces an adaptive covering, refining those boxes in particular that contribute to the error in computing the transport rates. Moreover, the algorithm gives an upper and lower bound to the transport rate, at least up to the error estimated in Lemma 4.2. Note that the numerical effort to compute the approximate transport rates essentially consists in n matrix-vector-multiplications – where the matrix $P_{\mathcal{B}}$ is sparse.

Transport Probabilities. In many applications one is interested in transport probabilities rather than in the transported volume. The transport probability as a function of the number of iterations n is given by

$$q_{i,j}(n) = \frac{T_{i,j}(n)}{m(R_i)},$$

that is, the fraction of particles in R_i that gets transported to R_j in n steps.

An approximation $\tilde{q}_{i,j}(n)$ to this quantity can be obtained using the upper and lower bounds on the transport rates and taking an average in the following way:

$$\tilde{q}_{i,j}(n) = \frac{\underline{T_{i,j}(n)} + \overline{T_{i,j}(n)}}{m(\underline{R_i}) + m(\overline{R_i})}.$$

Note that the quantities $\tilde{q}_{i,j}(n)$ can be computed from the box covering and the transition matrix, whereas in our setting the true transport probabilities $q_{i,j}(n)$ are theoretical values. Convergence of $\tilde{q}_{i,j}(n)$ to $q_{i,j}(n)$ follows from the results above when the box covering is appropriately refined.

4.3 Implementation

The algorithms described above are implemented in the dynamical systems software package GAIO (*Global Analysis of Invariant Objects*, see Dellnitz, Froyland, and Junge [2001]). The box collections $\mathcal{B}_k$ are realized by generalized rectangles of the form

$$B(c, r) = \{y \in \mathbb{R}^d \mid |y_i - c_i| \leq r_i \text{ for } i = 1, \ldots, d\},$$

where $c \in \mathbb{R}^d$ denotes the center and $r \in \mathbb{R}^d$ the radius of the rectangle (box). For our computations we use a finite number of test points in each box, such as a regular grid or Monte Carlo points; see for instance Dellnitz and Hohmann [1996] or Junge [1999] for a discussion on the choice of test points. In GAIO, the boxes are stored in a binary tree, where the children of a box at depth k are constructed by bisecting the box in alternate coordinate directions.

Note that the methods described above can be used in parallel to speed up the computation time.

5 Examples

We demonstrate the strength of our methods by computing ionization probabilities for the full and half scattering problems of the Rydberg atom in crossed electric and magnetic fields. We choose an energy of $E = -1.52$.

First we consider the full scattering problem of the 2-degree of freedom system for an electric field parameter $\epsilon = 0.57765$. We compare the results of the computation with the respective results for the 3-degree of freedom system. Then we analyze the 3-degree of freedom system for $\epsilon = 0.58$, allowing a comparison with Gabern, Koon, Marsden, and Ross [2005]. Finally, we use the results from the previous computations to consider the half scattering problem.

5.1 Full Scattering Problem for the 2- and 3-degree of Freedom System ($\epsilon = 0.57765$)

For the 2-degree of freedom system we consider the rectangle $X = [-0.295, -0.005] \times [-1.0, 1.0]$ on the Poincaré section Σ. We start with a partition of X on depth 8. By applying the return time algorithm in forward and backward time, we can identify and approximate the first stable and unstable tube intersections, respectively. As a result, we obtain a covering of X on depth 8, with the boxes covering the boundary of the tube intersections on depth 18. This covering consists of 736 boxes. We denote by $\underline{R_1}$ the set of boxes in the interior of the unstable tube intersection and by $\overline{R_1}$ the boxes covering the interior and the boundary. The sets $\underline{R_2}$ and $\overline{R_2}$ correspond to the stable tube intersection. Note that we are not given R_1 and R_2 explicitly because we can only approximate these sets on the box level, yielding $\underline{R_1}, \overline{R_1}, \underline{R_2}, \overline{R_2}$.

We then apply $J = 5$ steps of the adaptive refinement algorithm with 25 grid points per box. We choose $N = 5$ because we want to consider at least $n = 10$ iterations of the Poincaré map for our transport calculations. In each step, we subdivide in both coordinate directions at once. As the boundary is on depth 18, there is no gain in considering boxes on finer levels because while the computational effort increases, we would not get any new information. So the resulting box covering (18670 boxes), with those boxes contributing to the error in the transport rate having being refined, is on depth 8/18; see Figure 5.1.

In Figure 5.2 we show the numerical lower and upper bounds on the transport rates, $\underline{T_{1,2}(n)}$ and $\overline{T_{1,2}(n)}$ respectively, for $n = 1, \ldots, 15$. Observe that the scattering profile is structured. The approximate scattering probabilities $\tilde{q}_{1,2}(n)$ are shown in Figure 5.3(a). The electron scattering probability is about 22% for $n = 5$ loops around the nuclear core. It is zero or almost zero for all other n apart from $n = 10$ and $n = 11$, where we observe small probabilities.

To check the results, we computed these probabilities using as many as 900 grid points per box, obtaining almost identical results. So for the given accuracy of the sets of interest we can be sure that the results are correct.

We compare the results in the planar Rydberg system with those obtained in the 3-degree of freedom problem. In the 3-degree of freedom system we have the coordinates $x, y, z, \dot{x}, \dot{y}, \dot{z}$. Fixing a constant energy and a Poincaré section defined by (3.2), our remaining coordinates are $x, z, \dot{x}, \dot{z}$. Therefore, the initial box needs to be four-dimensional. For the following computations we chose $X = [-0.3, 0] \times [-0.1, 0.1] \times [-1.0, 1.0] \times [-2.0, 2.0]$.

We start with a box covering on depth 16 and apply the return time algorithm in forward and backward time which yields a covering of the boundaries of R_1 and R_2 on depth 36. The resulting box collection consists of 139276 boxes. We then apply $J = 7$ steps of the adaptive refinement algorithm, choosing $N = 5$ and 100 Monte Carlo points per box. In each step we subdivide in two coordinate directions at once and obtain a covering of 2056672 boxes, again on depth 16/36. The approximate electron scattering probabilities $\tilde{q}_{1,2}(n)$ for the full scattering problem are shown in Figure 5.3(b). Note that the scattering profile has the same qualitative characteristics as for the 2-degree of freedom system. Yet, the probabilities are lower

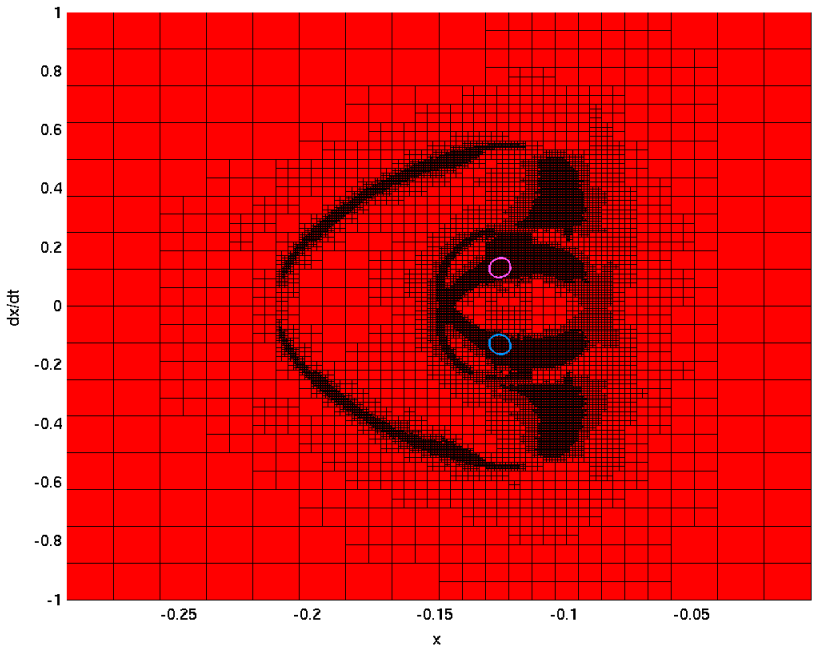

Figure 5.1: Adaptive box covering for the Rydberg atom in crossed fields. In the 2-degree of freedom system for $\epsilon = 0.57765$ those boxes are refined that contribute to the error in the computation of the transport rates. The unstable (light red) and stable (light blue) tube intersections are superimposed.

than in the planar case. A reason for this might be that the volumes of the tubes are smaller while the relative box sizes are considerably bigger than in the planar case. If the volume of the tube is comparatively small, as in our example, we need to use a box covering on a much deeper level to decrease the error between the upper and lower bounds of the transport rates. However, by doing this we obtain a covering that is hardly manageable because it consists of a huge number of boxes.

To verify our results for this parameter value we computed the transport probabilities in the 3-degree of freedom system using as many as 1000 Monte Carlo points per box. This computation confirmed our results. Furthermore, in the 2-degree of freedom system our results agree very well with calculations done for this value of ϵ by the authors of Gabern, Koon, Marsden, and Ross [2005] (personal communication).

5.2 Full and Half Scattering Problem for the 3-degree of Freedom System ($\epsilon = 0.58$)

Choosing $\epsilon = 0.58$, the first intersections of the stable and unstable tubes with the Poincaré surface overlap. For the computation of the electron scattering probabili-

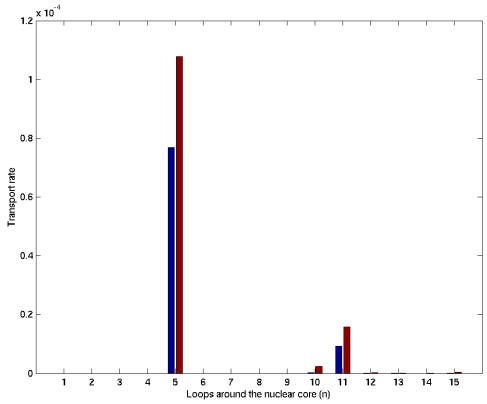

Figure 5.2: Full scattering problem for the 2-degree of freedom Rydberg atom in crossed fields for $\epsilon = 0.57765$. Approximation of the lower bound $\underline{T_{1,2}(n)}$ (blue) and the upper bound $\overline{T_{1,2}(n)}$ (red) on the transport rate for $n = 1, \ldots, 15$ is shown.

ties in the 3-degree of freedom system we consider a partition of X as defined above. The box covering consists of 2155528 boxes on depth 16/28, with the transport boxes refined using $J = 4$ steps of the adaptive algorithm as described above.

The scattering probabilities $\tilde{q}_{1,2}(n)$ with $n = 1, \ldots, 10$ are shown in Figure 5.4(a). These results compare well with the scattering probabilities obtained by Gabern, Koon, Marsden, and Ross [2005], who analyzed the system using the same parameters.

In addition, we can re-use the box covering and the transition matrix already computed for dealing with the half scattering problem.

Here we define $\underline{R_3} = X \setminus \overline{R_2}$ and $\overline{R_3} = X \setminus \underline{R_2}$, that is, we consider the transport of particles from every region outside the stable tube R_2 into R_2. Note that by this construction $\overline{R_2}$ and $\overline{R_3}$ have a non-empty intersection, containing the boundary boxes of R_2. So $\underline{T_{3,2}(n)}$ and $\overline{T_{3,2}(n)}$ can only give very coarse estimates on the transport rate because the boundary boxes are taken into account twice. Therefore we compute an approximation of the half scattering probability by

$$\hat{q}_{3,2}(n) = \frac{\underline{e_2}^T P_{\mathcal{B}}^n \overline{u_3} + \overline{e_2}^T P_{\mathcal{B}}^n \underline{u_3}}{m(\underline{R_3}) + m(\overline{R_3})}.$$

This represents an average of the transport from $\overline{R_3}$ to $\underline{R_2}$ and $\underline{R_3}$ to $\overline{R_2}$. The results are presented in Figure 5.4(b). Note that for higher iterates one observes an exponential decay of the electron scattering probabilities. Jaffé, Farrelly, and Uzer [1999] used a similar parameter value for the computation of so-called survival probabilities for the two-degree of freedom half scattering problem in their paper. Even if it is not exactly the same value (they used an electric field parameter of $\epsilon = 0.6$) the shapes of the probabilities for both ϵ values look qualitatively the same.

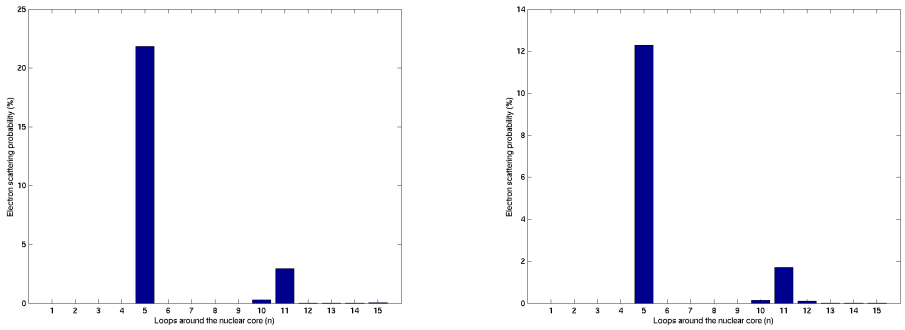

(a) (b)

Figure 5.3: Full scattering problem for the Rydberg atom in crossed fields for $\epsilon = 0.57765$. Approximate transport probabilities $\tilde{q}_{1,2}(n)$ for $n = 1, \ldots, 15$ in (a) the 2-degree of freedom system and (b) the 3-degree of freedom system.

6 Conclusion

This paper has presented a set oriented method for computing transport rates. We considered a suitable Poincaré section and introduced a new method for the computation of tube intersections with this section using the Poincaré first return time. Based on these intersections we have the necessary information to find the regions between which transport will occur. We can use an adaptive algorithm for the computation of the transport rates relevant for the present situation (see Dellnitz, Junge, et al. [2005] and Padberg [2005]). It focuses on a global description of the dynamics using a box covering of the interesting region and a matrix of transition probabilities between these boxes for the calculation of the transport rates.

These techniques were demonstrated in the 2- and 3-degree of freedom systems for the Rydberg atom in crossed electric and magnetic fields. The generalization to higher dimensions is straightforward with the limitation being the time taken to do the computations as well as the memory which would be required.

In contrast to Gabern, Koon, Marsden, and Ross [2005], the set oriented approach does not require normal form techniques for the computation of tube intersections and does not use a Monte Carlo approach for the computation of the reaction rates. However, there is agreement between the results of the two approaches.

One possible next step in this line of research is to experimentally verify the numerical results presented in this paper. The techniques for calculating the relevant transition rates are available but these observations have not yet been made. In such an experiment, there would be a spread of energies of the incoming electrons and also a variation in the electric field parameter ϵ. Thus, results of physical

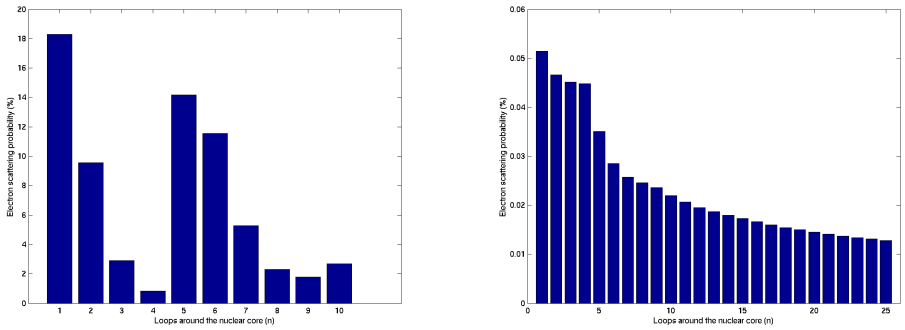

(a) (b)

Figure 5.4: The 3-degree of freedom Rydberg atom in crossed fields for $\epsilon = 0.58$. Approximation of transport probabilities in (a) the full scattering problem and (b) the half scattering problem.

observations would not exactly match those in Figure 5.3 and Figure 5.4 but should be qualitatively the same. That is, an experiment should look for a nonexponential structure in the ionization rate that resembles those calculated in this paper. For the results presented in this paper to be directly comparable with experimental results, we would need to average over both the energy and the electric field.

An ongoing priority is to make set oriented calculations in higher dimensional problems more computationally efficient. At the same time, methods to reduce the number of variables needed to describe the coarse dynamics of a high dimensional system are being pursued. The aim is to investigate high dimensional multiscale problems by combining the set oriented method with an appropriate procedure for distinguishing between optimal coarse and fine variables.

The methods presented in this paper represent a good starting point for further investigations that use dynamical systems and geometric observations combined with set oriented methods and statistics. To the best of our knowledge the results of this paper and those of Gabern, Koon, Marsden, and Ross [2005] represents the first successful calculation of reaction rates in a 3-degree of freedom chemical system.

Of course we also want to eventually apply these methods to the computation of reaction rates and transition probabilities for more complex molecules, such as to isomerization and conformations. To do so will surely require some form of model reduction and the associated identification of suitable reaction coordinates, with the methods of this paper applied to the coarse level dynamics. An interesting start on such an endeavor using the Perron-Frobenius eigenfunctions themselves as coarse variables has been given in Junge, Marsden, and Mezic [2004] and Nadler, Lafon, Coifman and Kevrekidis [2004]. Thus, we are quite hopeful that the techniques of this paper will be applicable to more complex problems.

Acknowledgements

The authors thank Frederic Gabern, Oliver Junge, Wang S. Koon and Shane D. Ross for helpful discussions and comments.

This work was partly supported by the German Science Foundation (DFG) Project SFB-376, the DFG Priority Program 1095, a Max Planck Research Award, and ARO grant DAAD19-03-D-0004 through the Santa Barbara ICB.

References

Ahn, J., D. N. Hutchinson, C. Rangan, and P. H. Bucksbaum [2001], Quantum phase retrieval of a Rydberg wave packet using a half-cycle pulse. *Phys. Rev. Lett.* **86**, 1179–1182.

Conley, C.C. [1968], Low energy transit orbits in the restricted three-body problem. *SIAM J. Appl. Math.* **16**(4), 732–746.

Contopoulos, G., and K. Efstathiou [2004], Escapes and recurrence in a simple hamiltonian system. *Celestial Mechanics and Dynamical Astronomy* **88**, 163–183.

De-Hua, Wang, and Lin Sheng-Lu [2004], Semiclassical calculation of the recurrence spectra of He Rydberg atom in perpendicular electric and magnetic fields. *Chinese Physics* **13**(4), 464–468.

De Leon, N., M.A. Mehta, and R.Q. Topper [1991], Cylindrical manifolds in phase space as mediators of chemical reaction dynamics and kinetics. I. Theory. *J. Chem. Phys.* **94**(12), 8310–8328.

De Leon, N., M.A. Mehta, and R.Q. Topper [1991], Cylindrical manifolds in phase space as mediators of chemical reaction dynamics and kinetics. II. Numerical considerations and applications to models with two degrees of freedom. *J. Chem. Phys.* **94**(12), 8329–8341.

De Leon, N. [1992], Cylindrical manifolds and reactive island kinetic theory in the time domain. *J. Chem. Phys.* **96**(1), 285–297.

Dellnitz, M., G. Froyland, and O. Junge [2001], The algorithms behind GAIO – Set oriented numerical methods for dynamical systems, in *Ergodic Theory, Analysis, and Efficient Simulation of Dynamical Systems* (ed. B. Fiedler), Springer, 145–174.

Dellnitz, M. and A. Hohmann [1996], The computation of unstable manifolds using subdivision and continuation, in *Nonlinear Dynamical Systems and Chaos* (eds. H.W. Broer, S.A. van Gils, I. Hoveijn, and F. Takens), PNLDE 19, Birkhäuser, 449–459.

Dellnitz, M. and A. Hohmann [1997], A subdivision algorithm for the computation of unstable manifolds and global attractors. *Numerische Mathematik* **75**, 293–317.

Dellnitz, M. and O. Junge [2002], Set oriented numerical methods for dynamical systems, in *Handbook of Dynamical Systems II: Towards Applications* (eds. B. Fiedler, G. Iooss and N. Kopell), World Scientific, 221–264.

Dellnitz, M., O. Junge, W.-S. Koon, F. Lekien, M. W. Lo, J. E. Marsden, K. Padberg, R. Preis, S. D. Ross and B. Thiere [2005], Transport in dynamical astronomy and multibody problems. *International Journal of Bifurcation and Chaos* **15**, in press.

Federov, M. V., and M. Yu. Ivanov [1990], Coherence and interference in a Rydberg atom in a strong laser field: excitation, ionization, and emission of light. *J. Opt. Soc. Am. B.* **7**(4), 569–573.

Gabern, F., W.S. Koon, J.E. Marsden, and S.D. Ross [2005], Theory and computation of non-RRKM lifetime distributions and rates in chemical systems with three or more degrees of freedom. (Submitted for publication).

Gilbert, R.G., and S.C. Smith [1990], *Theory of Unimolecular and Recombination Reactions*, Blackwell, Oxford.

Guckenheimer, J., and P. Holmes [1983], *Nonlinear Oscillations, Dynamical Systems, and Bifurcations of Vector Fields*. Springer Verlag, New York.

Held, H., J. Schlichter, G. Raithel, and H. Walther [1998], Observation of level statistics and Heisenberg-time orbits in diamagnetic Rydberg spectra. *Europhysics Letters* **43**(4), 392–397.

Jaffé, C., D. Farrelly, and T. Uzer [1999], Transition state in atomic physics. *Physical Review A* **60**(5), 3833–3850.

Junge, O. [1999], *Mengenorientierte Methoden zur numerischen Analyse dynamischer Systeme*. Ph.D. thesis, University of Paderborn.

Junge, O., J. E. Marsden, and I. Mezic [2004], Uncertainty in the dynamics of conservative maps, *Proc CDC* **43**, 2225–2230.

Koon, W.S., M.W. Lo, J.E. Marsden, and S.D. Ross [2000], Heteroclinic connections between periodic orbits and resonance transitions in celestrial mechanics. *Chaos* **10**(2), 427–469.

Marmet, L., H. Held, G. Raithel, J.A. Yeazell, and H. Walther [1994], Observation of quasi-Landau wave packets. *Phys. Rev. Lett.* **72**(24), 3779–3782.

Marston, C.C., and N. De Leon [1989], Reactive islands as essential mediators of unimolecular conformational isomerization: A dynamical study of 3-phospholene. *J. Chem. Phys.* **91**(6), 3392–3404.

McGehee, R. [1969], Some homoclinic orbits for the restricted three-body problem. *Ph.D. thesis*, University of Wisconsin, Madison.

Mezić, I., and S. Wiggins [1999], A method for visualization of invariant sets of dynamical systems based on the ergodic partition. *Chaos* **9**(1), 213–218.

Nadler, B, S. Lafon, R. Coifman and I. G. Kevrekidis [2004], Diffusion maps, spectral clustering and the reaction coordinates of dynamical systems (preprint).

Padberg, K. [2005], *Numerical Analysis of Transport in Dynamical Systems*. Ph.D. thesis, University of Paderborn.

Raithel, G., M. Fauth, and H. Walther [1991], Quasi-Landau resonances in the spectra of rubidium Rydberg atoms in crossed electric and magnetic fields. *Phys. Rev. A* **44**(3), 1898–1909.

Raithel, G., and H. Walther [1994], Ionization energy of rubidium Rydberg atoms in strong crossed electric and magnetic fields. *Phys. Rev. A* **49**(3), 1646–1665.

Truhlar, D.G., B.C. Garrett, and S.J. Klippenstein [1996], Current status of transition-state theory. *J. Phys. Chem.* **100**(31), 12771–12800.

Uzer, T., C. Jaffé, J. Palacián, P. Yanguas, and S. Wiggins [2002], The geometry of reaction dynamics. *Nonlinearity* **15**(4), 957–992.

Wojcik, A., and R. Parzynski [1995], Dark-state effect in Rydberg-atom stabilization. *J. Opt. Soc. Am. B.* **12**(3), 369–376.